

Evan Haas* and Frank De Luccia
The Aerospace Corporation, El Segundo CA

1. INTRODUCTION

The Visible Infrared Imaging Radiometer Suite (VIIRS) on the Suomi National Polar Orbiting Partnership (SNPP) satellite collects radiometric and imagery data in 22 spectral bands within the visible and infrared region ranging from 0.4 to 12.5 μm . The satellite is polar-orbiting, sun-synchronous, with 14.2 orbits per day. VIIRS spectral data are calibrated and geolocated in ground processing to generate Sensor Data Records (SDRs). The VIIRS instrument has a rotating telescope assembly (RTA) that allows it to continuously collect data from the Earth view and several other calibration views. A full rotation of the VIIRS instrument is completed every 1.79 seconds, and a half-angle mirror (HAM) rotates at half the rate of the RTA to direct light into stationary optics and focal plane arrays.

14 of the spectral bands are reflective solar bands (RSB) that are calibrated once per orbit by solar light passing through a solar attenuation screen (SAS) and reflected off of a solar diffuser (SD). An illustration of the VIIRS sensor with the SD and SAS is shown in figure 1. The ratio of the calculated to measured solar diffuser radiance is called the F factor, and is trended during the mission. A complete discussion of RSB calibration and the F factor can be found in Cardema (2012).

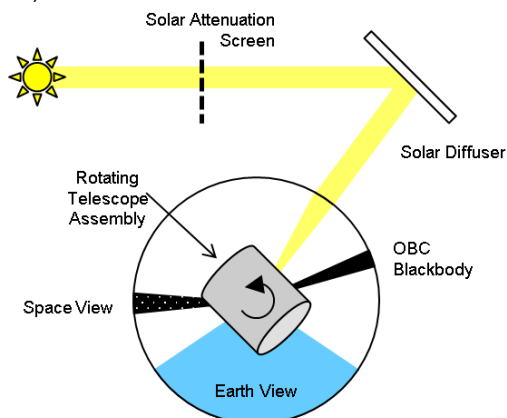


Figure 1. Illustration of the VIIRS RTA with associated views and solar calibration hardware.

The radiance when viewing the SD is a function of the SDS transmission and the SD's Bidirectional Reflectance Distribution Function (BRDF). The BRDF of the SD is expected to change throughout the mission, and the overall scale factor of this change is tracked and called the H factor. For a complete discussion of the H factor, see Haas (2012).

* Corresponding author address: Evan M. Haas, The Aerospace Corporation, P.O. Box 92957, M4/895, Los Angeles, CA 90009-2957; e-mail: Evan.M.Haas@aero.org

On-orbit changes in the H factor are monitored by a separate on-board instrument called the solar diffuser stability monitor (SDSM). It has been used during times of RSB calibration data collection at various frequencies throughout the mission (once per orbit to start, then reduced to once per day, and now 3 times per week). During a VIIRS scan, when the SDSM is operational, the SDSM collects 5 samples in one of 3 views: solar, SD, and dark reference. The SDSM is illustrated in figure 2. During a solar view, an attenuation screen called the SDSM screen reduces incoming solar radiance to levels comparable to those seen by the VIIRS sensor itself. During an SD view, the SDSM views the SD and the radiance is a function of the SAS transmission and the BRDF of the SD.

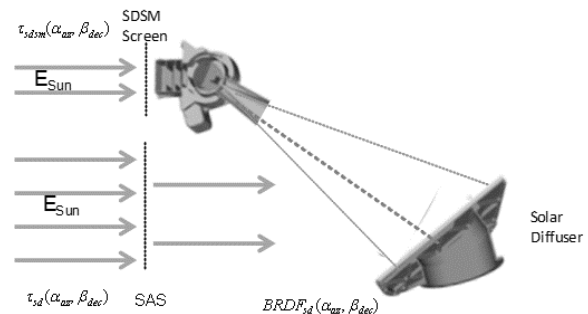


Figure 2. Illustration of the SDSM with solar and SD views.

Both the H and F factors are routinely trended as part of RSB calibration. This paper addresses unexpected trend changes that occurred in both the H and F factors in February and May of 2014. To understand the problem, we must develop the equations for each Factor. For the H factor, first we must define the gain of an SDSM detector when viewing the SD, given by equation 1:

$$G_{sd} = \frac{DC_{sd} - DC_{bkg}}{E_{sun} \cdot \tau_{sd}(\alpha_{az}, \beta_{dec}) \cdot \cos AOI_{sd} \cdot H \cdot BRDF(\alpha_{az}, \beta_{dec}) \cdot \sin^2(FOV_{sdsd})} \quad (1)$$

where DC_{sd} , and DC_{bkg} are the SDSM detector output digital counts from the SD and dark reference paths respectively, E_{sun} is the in-band solar irradiance at the satellite, $\tau_{sd}(\alpha_{az}, \beta_{dec})$ corresponds to the SDS transmittance as a function of solar azimuth α_{az} and declination β_{dec} , AOI_{sd} is the angle of incidence of sunlight on the SD, H is the BRDF degradation factor we seek to trend, $BRDF(\alpha_{az}, \beta_{dec})$ is the nominal BRDF as a function of solar angles, and FOV_{sdsd} is the fixed half cone angle of the SDSM field of view. Next, we can define the gain of an SDSM detector when viewing the sun, given by equation 2:

$$G_{sun} \frac{DC_{sun} - DC_{bkg}}{E_{sun} \cdot \tau_{ntn} \cdot \tau_{sdsm}(\alpha_{SDSMaz}, \beta_{SDSMel})} \quad (2)$$

where DC_{sun} is the SDSM detector output digital counts from the Solar path, τ_{ntn} is the SDSM screen transmittance at normal incidence, and $\tau_{sdsm}(\alpha_{SDSMaz}, \beta_{SDSMel})$ is the normalized SDSM screen transmittance, as a function of SDSM azimuth and SDSM elevation (transformed from solar azimuth and solar declination). Since the gains defined above are an intrinsic property of the SDSM and not a function of the source viewed, we can equate equations 2 and 3 and solve for the H factor, given in equation 3:

$$H = \frac{DC_{sd} - DC_{bkg}}{DC_{sun} - DC_{bkg}} \cdot \frac{\tau_{ntn} \cdot \tau_{sdsm}(\alpha_{az}, \beta_{dec})}{\tau_{sd}(\alpha_{az}, \beta_{dec}) \cdot \cos AOI_{sd} \cdot BRDF(\alpha_{az}, \beta_{dec}) \cdot \sin^2(FOV_{sdsm})} \quad (3)$$

Now, as mentioned before, the F factor is a ratio of calculated to measured radiance of the VIIRS instrument, given in equation 4:

$$F = \frac{L_{calc}}{L_{meas}} = \frac{P_{sun} \cdot \tau_{sd}(\alpha_{az}, \beta_{dec}) \cdot \cos(AOI_{sd}) \cdot H \cdot BRDF(\alpha_{az}, \beta_{dec})}{4 \cdot \pi \cdot d_{se}^2 \cdot (\sum_{i=0}^2 c_i (T_{det}, T_{elec}) \cdot dn^i)} \quad (4)$$

where L_{calc} is the calculated solar diffuser radiance, L_{meas} is the measured solar diffuser radiance, P_{sun} is the spectral solar power of the sun, $\tau_{sd}(\alpha_{az}, \beta_{dec})$ is the transmission of the solar diffuser screen, AOI_{sd} is the angle of incidence of sunlight on the solar diffuser, H is the H factor, $BRDF(\alpha_{az}, \beta_{dec})$ is the nominal BRDF as a function of solar angles, d_{se} is the earth-sun distance, dn is the offset corrected solar diffuser measured digital number, T_{det} is the detector temperature, T_{elec} is the electronics temperature, and c_i are temperature coefficients measured in pre-launch. H factors are not applied to the F factor as a per orbit calculated value, but rather a functional fit of the form $A \cdot \exp(B \cdot \text{orbit}) + C$ is applied to the H factor. Then, the fit is evaluated at the desired orbit to apply to the F factor. The product of the spectrally dependent terms in the calculated radiance is averaged over wavelength using the relative spectral response, but this detail is omitted here for simplicity. The band, detector, gain state, and HAM side dependence of the F factor is also suppressed in equation (4) for simplicity.

A trend change was first noticed in both H and F factors in March, 2014, roughly corresponding to orbit 12200. Figure 3 shows the operational H factors for each SDSM detector up to October 2014, roughly corresponding to orbit 15200. Table 1 shows the center wavelength (CW) for each SDSM detector and the corresponding nearest VIIRS band. In looking at the lower detectors, particularly detector 1, it is clear that the slopes of the trends changed prior to orbit 12000 and again near orbit 13000. In looking at equation 3, the cause of the trend change could be SDSM detector counts or any number of LUTs influenced by solar geometry.

At the same time the H factor trend change was noticed, a trend change was noticed in

the F factor as well. Figure 4 shows the F factor for band I1 (645nm CW). A distinct downward trend is noticed just prior to orbit 12000. This apparent trend change correlates well with the first noted trend change in H factor. The analysis of these trend changes along with mitigation for RSB calibration will be explored in this paper.

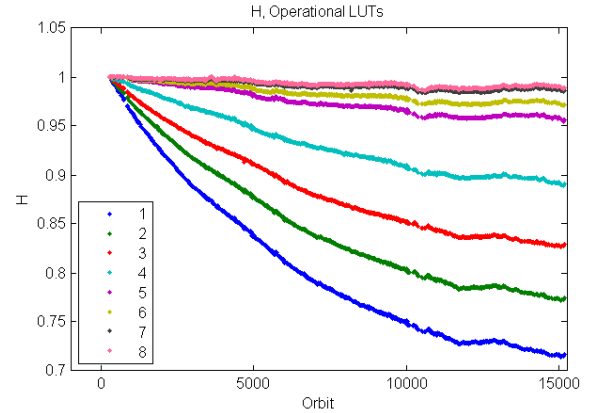


Figure 3. Operation H factors versus orbit up to October 2014. Trend changes can be noticed in detectors 1-4 near orbits 12000 and 13000.

SDSM Detector	CW* (μm)	VIIRS Bands	CW* (μm)
1	0.412	M1	0.412
2	0.450	M2	0.445
3	0.488	M3	0.488
4	0.555	M4	0.555
5	0.672	M5	0.672
6	0.746	M6	0.751
7	0.865	M7, I2	0.865
8	0.935	NA	NA

Table 1. Center wavelength of SDSM detectors with corresponding nearest VIIRS band.

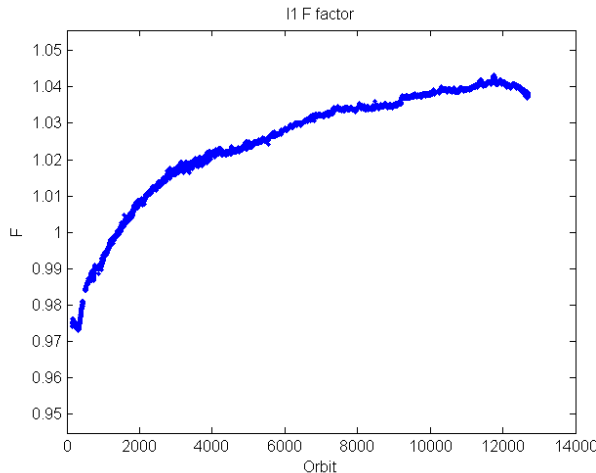


Figure 4. F factor versus orbit for band I1. A downward trend is noted just before orbit 12000.

2. H FACTOR TREND CHANGE

In order to better understand the H factor trend changes, pinpointing them in time was necessary. Prior to the first trend change, the H factor was fit with a global regression using all data from the mission history. The residual of the fit makes it apparent when the trend change began. Figure 5 shows the H factor fit residual zoomed to around the time of the first trend change. The residuals in all 8 SDSM bands peak at orbit 11746 (February 2, 2014), and then decrease. The residuals in all bands decrease, with residuals in shorter wavelength bands decreasing more. This behavior is consistent with the apparent flattening of H factors in shorter wavelengths seen in figure 3. Despite the clear peak in residuals, the exact orbit of the trend change cannot be determined due to uncertainty in the H factor. However, the steepness with which the residuals decrease after orbit 11746 is indicative of a rapid change.

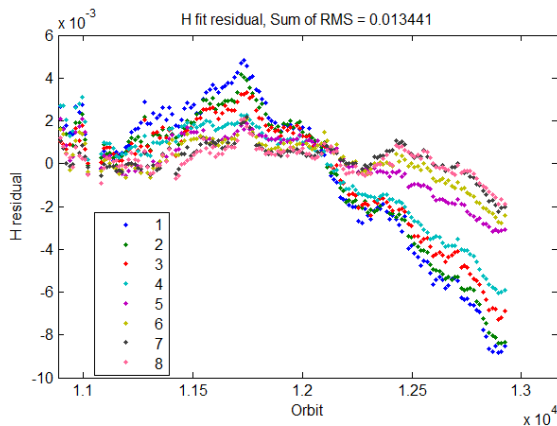


Figure 5. H factor fit residual for 8 SDSM bands. The peak in residuals is orbit 11746 (February 2, 2014).

Nothing out of the ordinary occurred for VIIRS or the spacecraft on February 2, 2014, however a petulant mode event did occur on February 4, 2014. The petulant mode is an instrument electronics related anomaly that causes shutdown and restart of VIIRS. Although the petulant mode event occurred near in time to the trend change, close examination of the H factor trends suggest that the petulant mode event occurred later than the trend change. The true time ordering of these events is somewhat uncertain due to H factor uncertainty, but the apparent time ordering raises doubt regarding any causal relationship between the petulant mode event and the trend change. Figure 6 shows a zoomed plot of the H factor for SDSM detector 1.

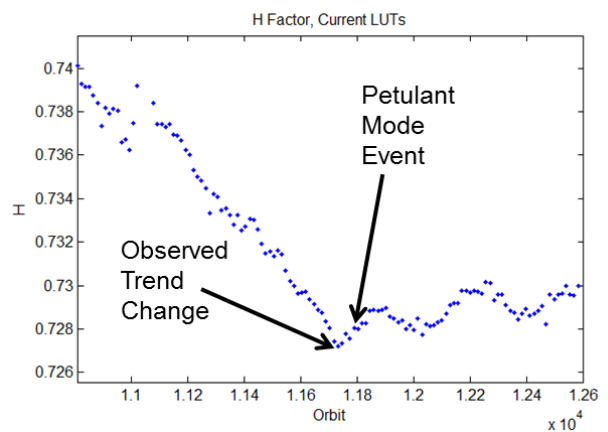


Figure 6. H factor for SDSM detector 1. The petulant mode event appears to occur after the observed trend change.

After the first trend change, the existing method of performing a global regression on H factors for application in F factors was not sufficient. The assumption that the H factor would follow a single trend over the mission history was violated by the abrupt change, so a new methodology needed to be applied. Beginning at orbit 11746, a second piecewise fit of the same form was applied to the H factor time series. The reasoning behind this decision was that the H factor seemed to experience a change within a day or so, and then continue on a new stable trend. Maintaining the same functional form allowed for easy integration into the existing F factor LUT delivery method. Also, this methodology gave the flexibility of applying as many piecewise fits as would be needed, should the trend change again.

A second H factor trend change occurred about 1000 orbits after the first trend change, as can be seen in figure 3. Pinpointing the time of the second trend change was done by applying the same method applied for the first: examination of the behavior of the H factor fit residuals. Figure 7 shows the fit residual zoomed around the time of the trend change. The local minimum before the residuals drastically

increase was at orbit 13207 (May 16, 2014). Once this trend change was identified, a third piecewise fit was applied starting at orbit 13207 for the purpose of applying H factors to F factors. To date, this third trend has continued without another change.

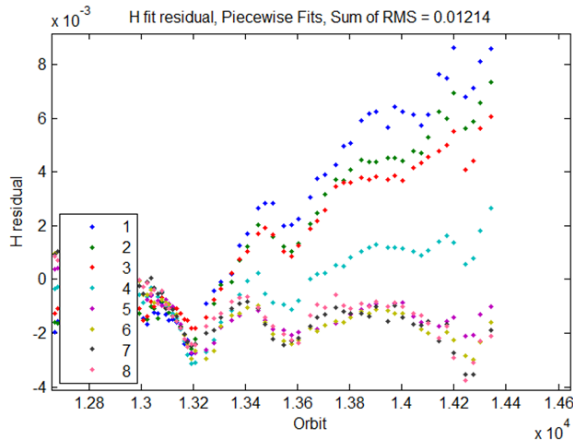


Figure 7. H factor fit residual for 8 SDSM bands. The trend change occurs at orbit 13207 (May 16, 2014).

In order to understand these trend changes further, the slopes before and after each trend change were compared for each SDSM detector. First, linear regressions were performed over 1000 orbits both before and after each trend change. Then, a slope difference was calculated as the prior slope minus the later slope for each trend change. Figure 8 shows the results. Blue dots represent the slope differences around the first trend change (orbit 11746) versus SDSM detector center wavelength, and red dots represent the slope differences around the second trend change (orbit 13207) versus SDSM detector center wavelength. First, we notice that slope differences have a spectral dependence. Also, we notice that slopes after orbit 13207 return very closely to slopes before orbit 11746. (The slope changes shown in figure 3 are approximately of the same magnitude but opposite sign for each wavelength.) This means that the third (and current) trend basically continued from where the first trend left off. Whatever caused the first trend change was reversed after 1461 orbits (102 days).

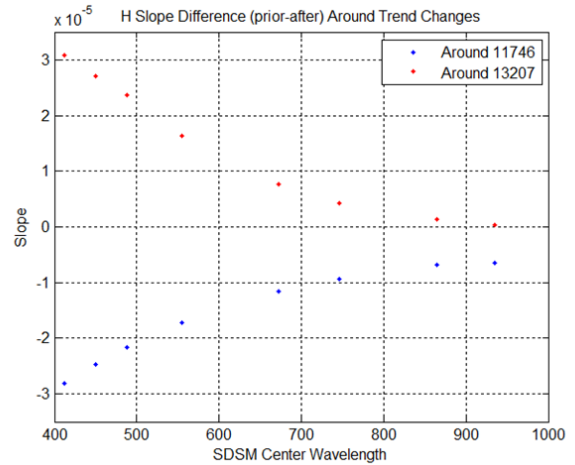


Figure 8. Slope difference (prior slope minus later slope) around each trend change.

To better understand the trend changes, looking at each input into the H factor calculation given in equation 3 is necessary. Many inputs to the H factor rely on solar geometry. Solar azimuth, solar elevation, SDSM azimuth, and SDSM elevation as functions of orbit are shown in figures 9-12, respectively. The former two angles are measured in the instrument coordinate system, while the latter two angles are measured in the SDSM coordinate system. The slopes of all of the plots look the same between the red lines indicating the times of the two trend changes as in corresponding time periods in prior years (to the left in the plots). Although the slopes do not appear to be different, one notices that the plateau in azimuth data is higher than in prior years. However, one would expect either a local slope or level change in these angles to occur if geometry change were a causal factor in the H factor trend change.

Since there were no changes in solar geometry coinciding with the trend changes, we need to look at the LUT outputs rather than the solar geometry inputs to determine if a trend change occurred in these outputs. Figure 13 shows the $T_{\text{sdsm}}(\alpha_{\text{SDSMz}}, \beta_{\text{SDSMdec}})$ values for the mission history for SDSM detector 1. Figure 14 shows the product $1/(T_{\text{sd}}(\alpha_{\text{az}}, \beta_{\text{dec}}) * \text{BRDF}(\alpha_{\text{az}}, \beta_{\text{dec}}))$ for the mission history for SDSM detector 1. Finally, figure 15 shows the $1/\cos(\text{AOI}_{\text{sd}})$ values over the mission history. There is nothing in these plots to suggest a trend change, just as there was nothing in the solar geometry plots to suggest a trend change.

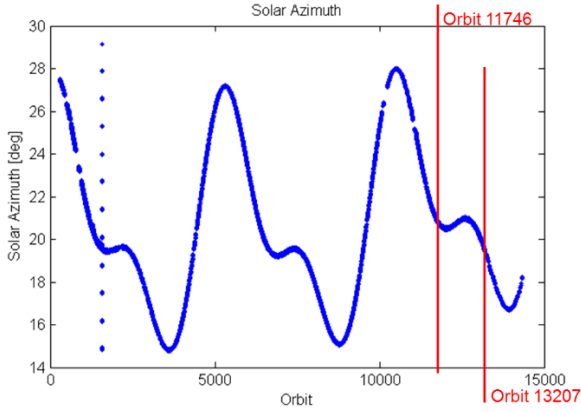


Figure 9. Solar Azimuth versus orbit over the mission history with trend change orbits annotated.

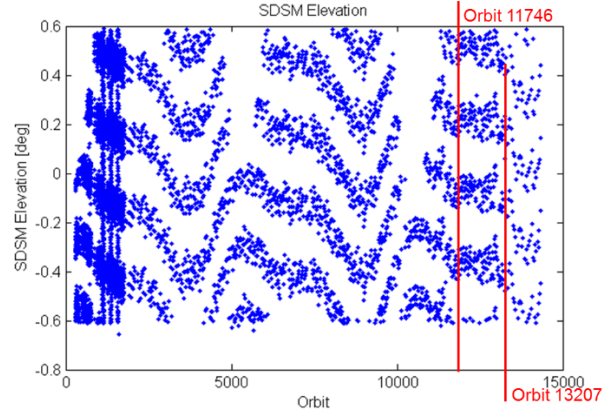


Figure 12. SDSM Elevation versus orbit over the mission history with trend change orbits annotated.

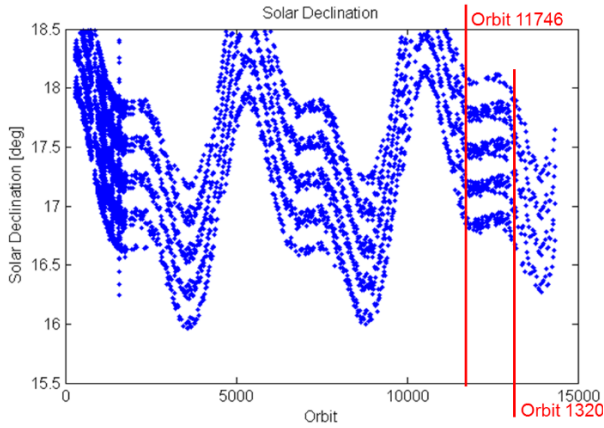


Figure 10. Solar Declination versus orbit over the mission history with trend change orbits annotated.

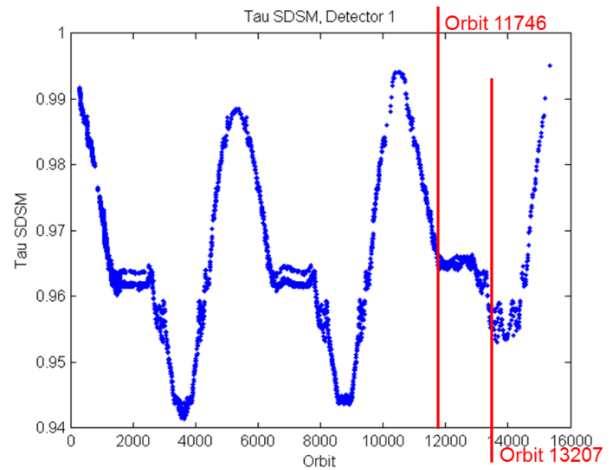


Figure 13. Operational $\tau_{sdsm}(\alpha_{SDSMz}, \beta_{SDSMdec})$ values versus orbit for SDSM detector 1.

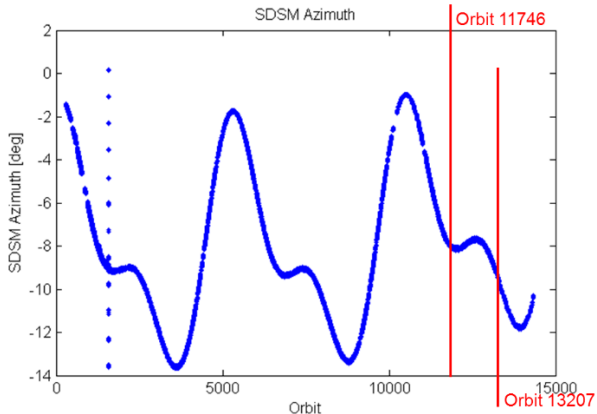


Figure 11. SDSM Azimuth versus orbit over the mission history with trend change orbits annotated.

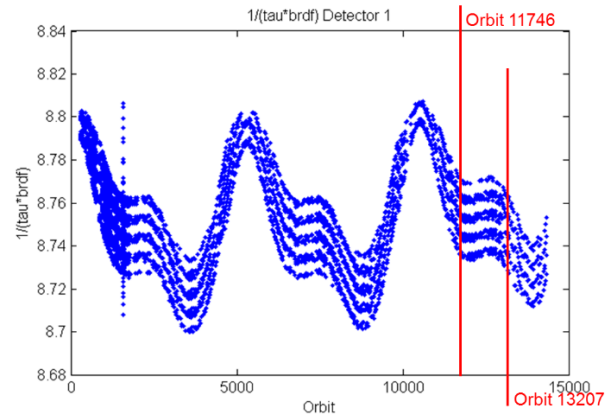


Figure 14. Operational $1/(\tau_{sd}(\alpha_{az}, \beta_{dec}) * BRDF(\alpha_{az}, \beta_{dec}))$ values versus orbit for SDSM detector 1.

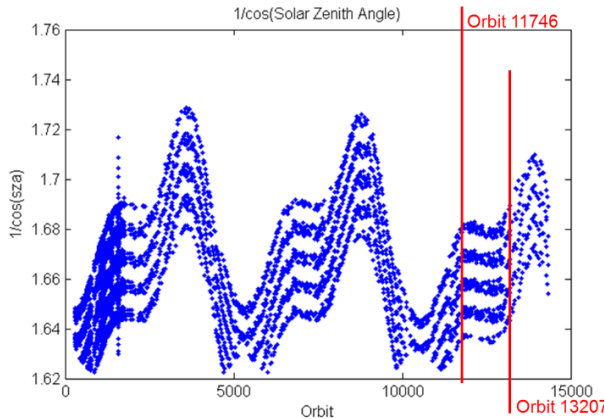


Figure 15. $1/\cos(\text{AOI}_{sd})$ (also called Solar Zenith angle) versus orbit over the mission history with trend change orbits annotated.

Since solar geometry values and associated LUT values did not seem to exhibit any trend changes, we next look to the SDSM output count (DC) values. Figure 16 shows the quantity $DC_{sd} - DC_{bkg}$ (denoted dc SD) for SDSM detector 1. Figure 17 shows the quantity $DC_{sun} - DC_{bkg}$ (denoted dc Sun) for SDSM detector 1. Figure 16 shows distinct trend changes right after each red line. The signal in previous years was very linear in the region after each local maximum, however the signal between the red lines deviates significantly. Now, looking at figure 17, we do not see a trend change between the red lines. This solar view signal is not as linear as the SD view, but one notices that the qualitative features present between the red lines match the features of the previous year's cycle very well. From these two plots we can conclude that the cause of the overall trend change in H factors can be isolated to the SD viewing path of the SDSM. Either the SD radiance or the SDSM responsivity or both must have changed in trend. Since SDSM measurements of the solar radiance are the same as before, it is highly unlikely that any trend change in SDSM responsivity occurred. Therefore, it follows that a change in SD radiance trend caused the H factor trend change.

A change in SD radiance trend can only be caused by a change in trend of the illumination of the SD or a change in the degradation rate of SD reflectance. Since abrupt trend changes in the solar illuminating geometry and in the SAS transmission have already been ruled out, the only remaining possible cause is a change in the degradation rate of SD reflectance. This conclusion will further be corroborated when looking at the F factor trends when the correctly fitted H factors are incorporated. It is important to note that there was no observed discontinuity in the offset corrected SDSM measurements for any SDSM detector, just a change in the rate of change of those

measurements. Equivalently, there was no evidence of an abrupt change in SD reflectance, just an abrupt change in the rate of change, or degradation rate, of the SD reflectance.

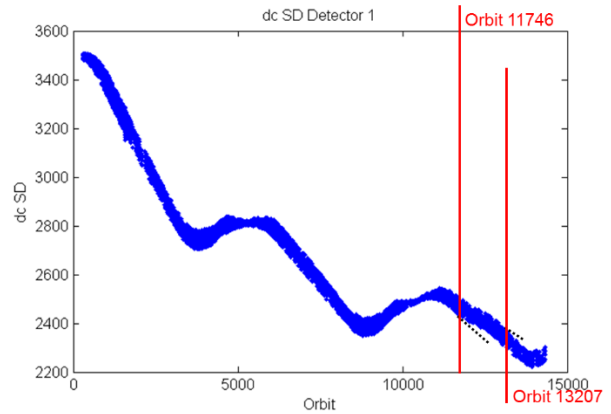


Figure 16. $DC_{sd} - DC_{bkg}$ (denoted dc SD), background subtracted SD view for SDSM detector 1. Dotted lines added to extend previous trends.

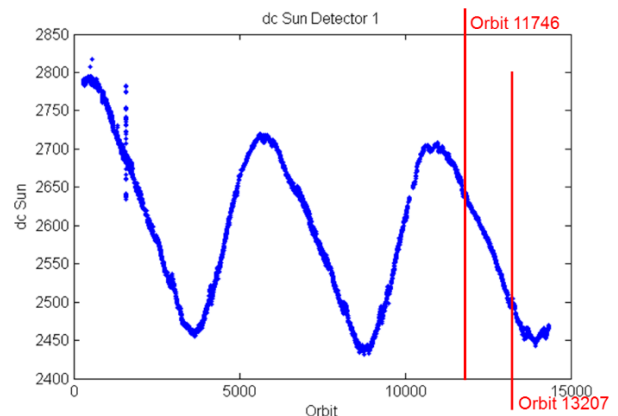


Figure 17. $DC_{sun} - DC_{bkg}$ (denoted dc Sun), background subtracted sun view for SDSM detector 1.

3. F FACTOR TREND CHANGE

Figure 4 shows the F factor for a band clearly affected by the first trend change. As discussed in the H factor trend change section, improper H factor values were being applied to this F factor. The H factor is now fit with three piecewise functions of the form $A \cdot \exp(B \cdot \text{orbit}) + C$, where the first fit captures all data prior to the first trend change, the second fit captures data between the first and second trend changes, and the third fit captures all data after the second trend change to present time. Figure 18 shows an example for VIIRS band M1, which has the same center wavelength as SDSM detector 1. Here we see the effects on F factor due to implementing the third piecewise fit of the H factor. When the second trend change occurred, but the correct H factor was not yet being applied, the F factor for M1

began to grow at a rate that was not typical for the past year. Applying corrected H factors reduced the growth in F factor significantly and produced a trend that was in family with the prior trend. The F factor trends for the remainder of the RSB calibrated VIIRS bands are shown in figures 19 through 31. For bands I1, I2, and M1-M7, time varying H factors are applied. For all other bands shown, H is set to 1 for all time because the SD does not appreciably degrade in those wavelengths.

After applying properly fitted H factors to F factors, there are no longer any noticeable trend changes in F factors near orbits 11746 and 13207. This finding further reinforces the notion that something caused a change in the rate of degradation of the SD. Since the F factor time series does have modulations in some bands that could disguise or "hide" a subtle trend change, a similar evaluation was performed for each input into the F factor equation as was done for the H factor. There were no noticeable trend changes in any inputs to the F factor at orbits 11746 and 13207. This finding is consistent with the finding of no observable trend changes in the F factor time series itself in any band, and again reinforces the notion that the only change in the system at these orbits was in the rate of change of the SD reflectance.

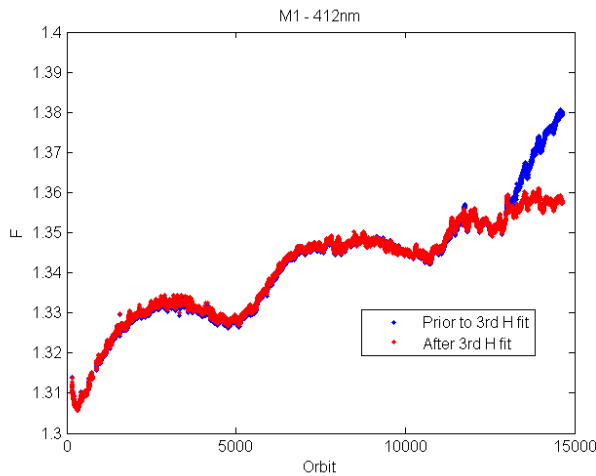


Figure 18. F factor for M1 before and after correction of the H factor using a third piecewise fit for H after the second trend change.

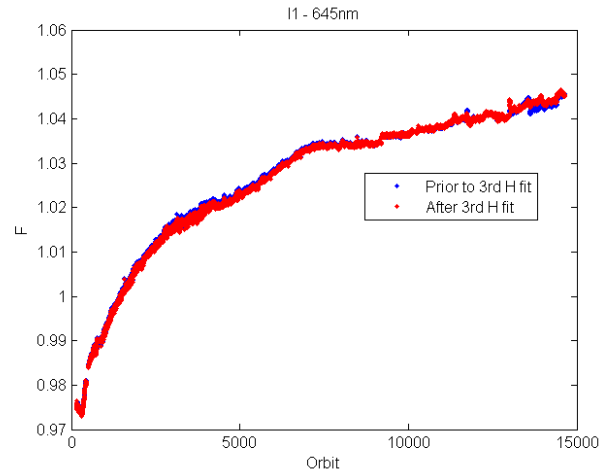


Figure 19. F factor for I1 before and after correction of the H factor using a third piecewise fit for H after the second trend change.

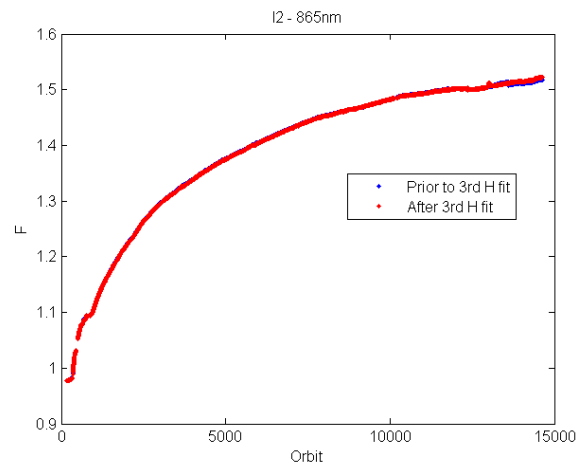


Figure 20. F factor for I2 before and after correction of the H factor using a third piecewise fit for H after the second trend change.

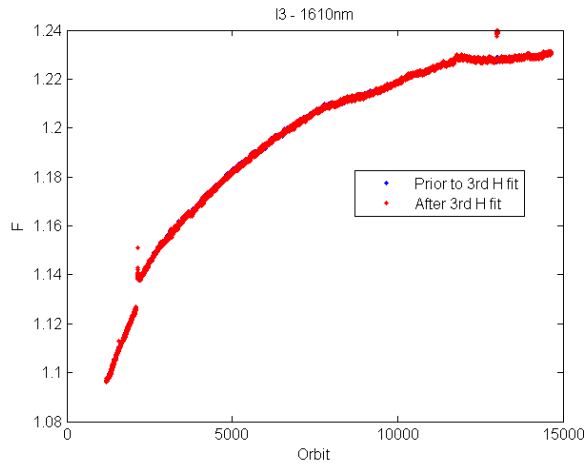


Figure 21. F factor for I3 before and after correction of the H factor using a third piecewise fit for H after the second trend change.

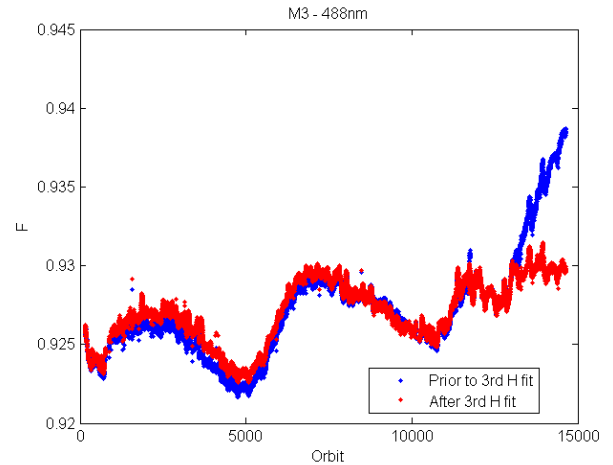


Figure 23. F factor for M3 before and after correction of the H factor using a third piecewise fit for H after the second trend change.

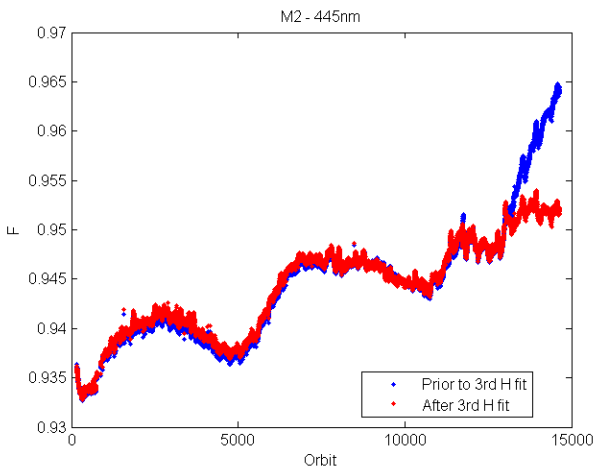


Figure 22. F factor for M2 before and after correction of the H factor using a third piecewise fit for H after the second trend change.

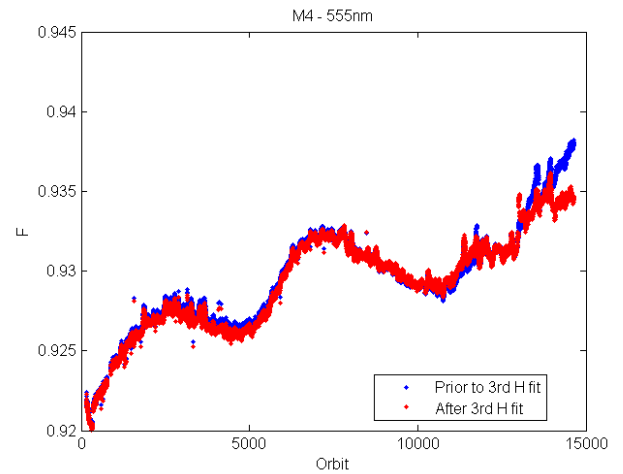


Figure 24. F factor for M4 before and after correction of the H factor using a third piecewise fit for H after the second trend change.

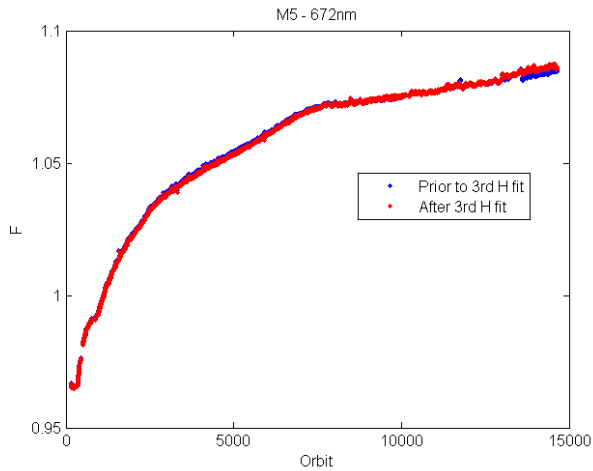


Figure 25. F factor for M5 before and after correction of the H factor using a third piecewise fit for H after the second trend change.

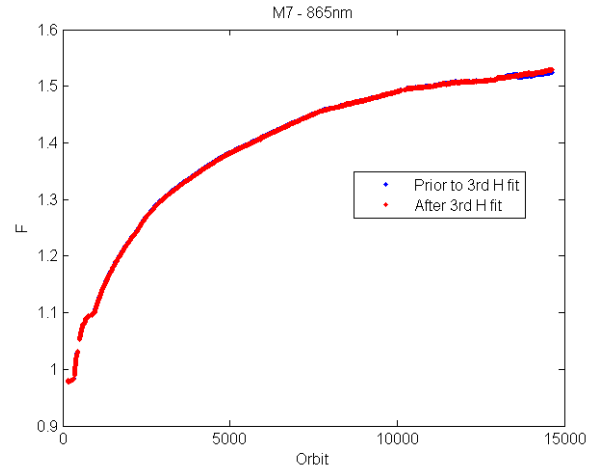


Figure 27. F factor for M7 before and after correction of the H factor using a third piecewise fit for H after the second trend change.

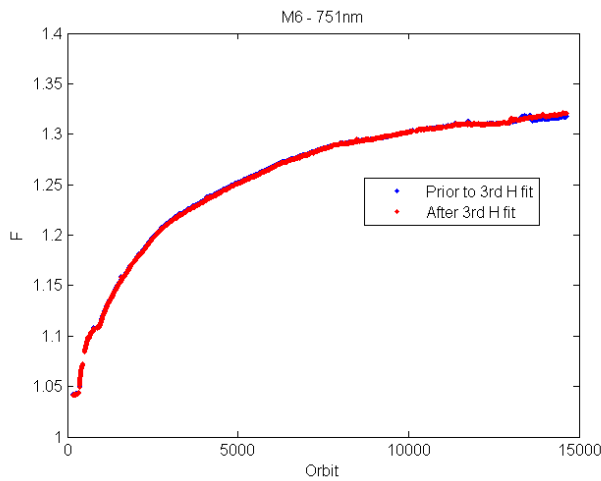


Figure 26. F factor for M6 before and after correction of the H factor using a third piecewise fit for H after the second trend change.

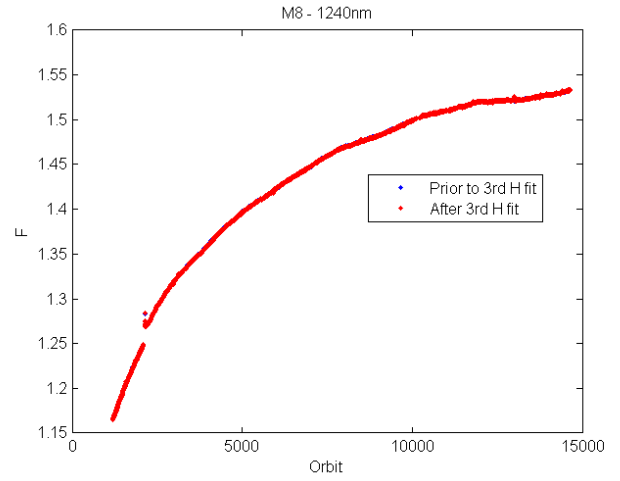


Figure 28. F factor for M8 before and after correction of the H factor using a third piecewise fit for H after the second trend change.

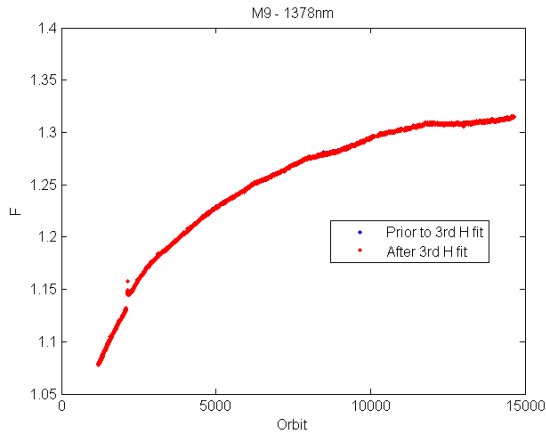


Figure 29. F factor for M9 before and after correction of the H factor using a third piecewise fit for H after the second trend change.

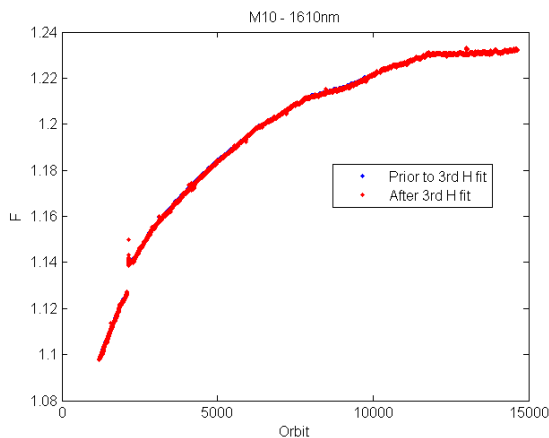


Figure 30. F factor for M10 before and after correction of the H factor using a third piecewise fit for H after the second trend change.

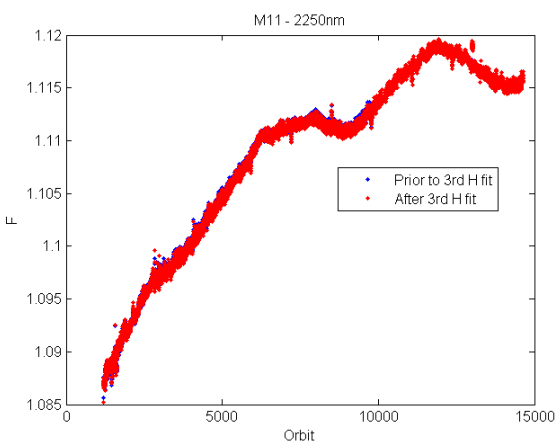


Figure 31. F factor for M11 before and after correction of the H factor using a third piecewise fit for H after the second trend change.

4. CONCLUSION

In early February of 2014, the H factor trends changed from their typical monotonically decreasing trends to a flat or slightly increasing trend. The trends for shorter wavelength SDSM detectors, which typically exhibit steeper downward trends than the longer wavelength detectors, changed the most. Then, in May of 2014, the H factor trends returned closely to their typical downward trends. These trend changes in the H factor can be traced to changes in the SDSM measurements of the solar diffuser radiance. Since the SDSM measurements of the solar radiance and other terms in the H factor equation did not change, the behavior of the solar diffuser reflectance must have changed. The SD reflectance degradation rate evidently decreased to produce the first trend change and then later increased to typical values to produce the second trend change. After applying a piecewise fitting scheme to the H factors for application in the F factors, the trend changes in the H factors were well represented. Resulting F factors do not exhibit any trend changes correlated with either the first or second H factor trend changes, suggesting that the only change to the system was in the rate of SD reflectance degradation.

At the time of this writing the cause of the SD reflectance degradation rate change is unknown. The close proximity in time of the trend change to a petulant mode event may or may not be related. The trend change appears to have occurred several days before the petulant mode event, but there is some uncertainty in pinpointing the onset of the first trend change. Also, many petulant mode events have occurred in the past with no apparent impact on H factor trends. Determination of the root cause of the H factor trend changes remains to be accomplished.

5. REFERENCES

Cardema, J., Rausch, K. Lei, N., Moyer, D., De Luccia, F., 2012: Operational Calibration of VIIRS Reflective Solar Band Sensor Data Records, Proceedings of SPIE Vol. 8510, 851019

Haas, E., Moyer, D., De Luccia, F., et al., 2012: VIIRS solar diffuser bidirectional reflectance distribution function (BRDF) degradation factor operational trending and update, Proceedings of SPIE Vol. 8510, 851016